Two-mode division multiplexing in a silicon-on-insulator ring resonator

Bryce A. Dorin* **and Winnie N. Ye**

Department of Electronics, Carleton University
1125 Colonel By Drive, Ottawa, ON K1S 5B6 Canada

*bdorin@doe.carleton.ca

Abstract: Mode-division multiplexing (MDM) is an emerging multiple-input multiple-output method, utilizing multimode waveguides to increase channel numbers. In the past, silicon-on-insulator (SOI) devices have been primarily focused on single-mode waveguides. We present the design and fabrication of a two-mode SOI ring resonator for MDM systems. By optimizing the device parameters, we have ensured that each mode is treated equally within the ring. Using adiabatic Bezier curves in the ring bends, our ring demonstrated a signal-to-crosstalk ratio above 18 dB for both modes at the through and drop ports. We conclude that the ring resonator has the potential for filtering and switching for MDM systems on SOI.

OCIS codes: (230.3120) Integrated optics devices; (230.5750) Resonators; (200.4650) Optical interconnects.

References and links

1. B. G. Lee, X. Chen, A. Biberman, X. Liu, I.-W. Hsieh, C.-Y. Chou, J. I. Dadap, F. Xia, W. M. J. Green, L. Sekaric, Y. a. Vlasov, R. M. Osgood, and K. Bergman, "Ultrahigh-Bandwidth Silicon Photonic Nanowire Waveguides for On-Chip Networks," IEEE Photon. Technol. Lett. **20**(6), 398–400 (2008).
2. D. Dai, J. Wang, and Y. Shi, "Silicon mode (de)multiplexer enabling high capacity photonic networks-on-chip with a single-wavelength-carrier light," Opt. Lett. **38**(9), 1422–1424 (2013).
3. R.-j. Essiambre, G. Kramer, P. J. Winzer, G. J. Foschini, and B. Goebel, "Capacity Limits of Optical Fiber Networks," J. Lightwave Technol. **28**(4), 662–701 (2010).
4. R. Ryf, S. Randel, A. H. Gnauck, C. Bolle, A. Sierra, S. Mumtaz, M. Esmaeelpour, E. C. Burrows, R.-j. Essiambre, P. J. Winzer, D. W. Peckham, A. H. Mccurdy, and R. Lingle, "Mode-Division Multiplexing Over 96 km of Few-Mode Fiber Using Coherent 6 x 6 MIMO Processing," J. Lightwave Technol. **30**(4), 521–531 (2012).
5. S. P. Chan, C. E. Png, S. T. Lim, G. T. Reed, and V. M. N. Passaro, "Single-Mode and Polarization-Independent Silicon-on-Insulator Waveguides With Small Cross Section," J. Lightwave Technol. **23**(6), 2103–2111 (2005).
6. P. Dumon, W. Bogaerts, V. Wiaux, J. Wouters, S. Beckx, J. V. Campenhout, D. Taillaert, B. Luyssaert, P. Bienstman, and D. V. Thourhout, "Low-Loss SOI Photonic Wires and Ring Resonators Fabricated With Deep UV Lithography," IEEE Photon. Technol. Lett. **16**(5), 1328–1330 (2004).
7. P. Dong, S. F. Preble, and M. Lipson, "All-optical compact silicon comb switch," Opt. Express **15**(15), 9600–9605 (2007).
8. Q. Xu, B. Schmidt, S. Pradhan, and M. Lipson, "Micrometre-scale silicon electro-optic modulator." Nature **435**, 325–327 (2005).
9. A. C. Ruege, S. Member, and R. M. Reano, "Sharp Fano Resonances From a Two-Mode Waveguide Coupled to a Single-Mode Resonator," J. Lightwave Technol. **28**(20), 2964–2968 (2010).
10. Y. Tanushi and S. Yokoyama, "Compact Multimode Optical Ring Resonators for Interconnection on Silicon Chips," Jpn. J. of Appl. Phys. **46**(4B), 2364–2368 (2007).
11. A. Vorckel, M. Monster, W. Henschel, P. H. Bolivar, and H. Kurz, "Asymmetrically Coupled Silicon-On-Insulator Microring Resonators for Compact Add-Drop Multiplexers," IEEE Photon. Technol. Lett. **15**(7), 921–923 (2003).
12. J. B. Driscoll, R. R. Grote, B. Souhan, J. I. Dadap, M. Lu, and R. M. Osgood, "Asymmetric Y junctions in silicon waveguides for on-chip mode-division multiplexing." Opt. Lett. **38**(11), 1854–1856 (2013).

#201705 - $15.00 USD Received 21 Nov 2013; revised 17 Jan 2014; accepted 19 Jan 2014; published 20 Feb 2014

13. T. Uematsu, Y. Ishizaka, Y. Kawaguchi, K. Saitoh, and M. Koshiba, "Design of a Compact Two-Mode Multi/Demultiplexer Consisting of Multimode Interference Waveguides and a Wavelength-Insensitive Phase Shifter for Mode-Division Multiplexing Transmission," J. Lightwave Technol. **30**(15), 2421–2426 (2012).
14. H. Qiu, H. Yu, T. Hu, G. Jiang, H. Shao, P. Yu, J. Yang, and X. Jiang, "Silicon mode multi/demultiplexer based on multimode grating-assisted couplers," Opt. Express **21**(15), 17904–17911 (2013).
15. Y. Ding, J. Xu, F. Da Ros, B. Huang, H. Ou, and C. Peucheret, "On-chip two-mode division multiplexing using tapered directional coupler-based mode multiplexer and demultiplexer," Opt. Express **21**(8), 10376 (2013).
16. M. Greenberg and M. Orenstein, "Multimode add-drop multiplexing by adiabatic linearly tapered coupling," Opt. Exp. **13**(23), 9381–9387 (2005).
17. A. Melloni, P. Monguzzi, R. Costa, and M. Martinelli, "Design of curved waveguides: the matched bend." J. Opt. Soc. Am. A **20**, 130–137 (2003).
18. L. Soldano and E. Pennings, "Optical multi-mode interference devices based on self-imaging: principles and applications," J. Lightwave Technol. **13**(4), 615–627 (1995).
19. L. H. Gabrielli, D. Liu, S. G. Johnson, and M. Lipson, "On-chip transformation optics for multimode waveguide bends." Nat. Commun. **3**, 1217 (2012).
20. M. Sumetsky, "Theory of adiabatic optical fiber and microfiber tapers," in "Optical Fiber Communication Conference and Exposition and The National Fiber Optic Engineers Conference," Technical Digest (CD) (Optical Society of America, 2006), paper OTuH2.
21. H. Yun, W. Shi, Y. Wang, L. Chrostowski, and N. A. F. Jaeger, "2 x 2 Adiabatic 3-dB Coupler on Silicon-on-Insulator Rib Waveguides," Proc. SPIE **8915** (2013).
22. D. Lancaster, "The Math Behind Bezier Cubic Splines," http://www.tinaja.com/glib/cubemath.pdf.
23. Y. Wang, J. Flueckiger, C. Lin, and L. Chrostowski, "Universal Grating Coupler Design," Proc. SPIE **8915** (2013).

1. Introduction

Silicon-on-insulator (SOI) wire waveguides have been identified to potentially replace copper wires for intra-chip communication. Developments in the fabrication of photonic integrated circuits are leading the way to making this vision a reality. To take advantage of the wide bandwidth of SOI waveguides, wavelength-division multiplexing (WDM) has been implemented, drastically increasing data transfer rates [1]. However, in SOI systems WDM does have inherent drawbacks, as it requires the operation and alignment of many individual laser sources. Another form of multiple-input multiple-output transmission is mode-division multiplexing (MDM), where channels are separated spatially by multiplexing them onto the different modes of a waveguide. The advantage of a MDM system is that it requires only one laser source to be coupled to the chip, which is then divided into N waveguides via a power splitter, and modulated using integrated silicon modulators [2]. As well, mode multiplexing in SOI has a huge advantage in terms of the utilization and manipulation of all supported modes for added functionalities without sacrificing device footprint. This is demonstrated in [2] where multiplexers are presented with lengths less than 100 μm for four modal channels. MDM is a viable alternative to WDM in multiple-input multiple-output photonic circuits on SOI, and presents advantages as it requires only one carrier wavelength to operate. MDM is also being aggressively pursued for fiber-optic telecommunications, where WDM has been tremendously successful but is beginning to reach spectral efficiency limits [3]. Recently, three modal channels were demonstrated in a fiber over a transmission distance of 96 km [4].

Single-mode operation has previously been regarded as an important design requirement for SOI waveguide-based devices [5]. Therefore, most optical devices designed in SOI are incompatible with MDM systems which require multimode waveguides. The ring resonator is an important device used for multiplexing, switching, and modulating in on-chip communications [6–8]. In [9] a multimode bus waveguide is coupled to a single-mode ring resonator, where both modes exhibited a resonance response. However, this device is not suitable for MDM applications as the fundamental mode of the single-mode ring resonator was excited regardless of input mode, therefore significant crosstalk between modes was found during resonance. In the past wide waveguides have been used in ring resonators for their ability to reduce propagation and bending loss for the fundamental mode [10]. The waveguide in these structures was

#201705 - $15.00 USD Received 21 Nov 2013; revised 17 Jan 2014; accepted 19 Jan 2014; published 20 Feb 2014

designed wide enough to be multimode when straight, but the authors ensured that the higher-order modes were lossy in the ring bends to avoid resonance of any mode but the TE_{00} for single-mode operation in the device. Such a device is also incompatible with MDM systems.

For the first time we demonstrate a ring resonator designed to support two modes, TE_{00} and TE_{01}, for MDM applications. Such a device could drastically increase the complexity and functionality of on-chip MDM communications by allowing for mode selective add/drop filtering. By adopting an active multimode ring resonator, mode selective switching and modulating could also be achieved [7, 8]. In this paper we outline the operation of a ring resonator composed of multimode waveguides, and present experimental results from fabricated devices. The design and optimization of the (de)multiplexers and ring bends are also reported.

2. Operation of a multimode ring resonator

A schematic detailing the proposed multimode ring resonator structure is shown in Fig. 1. The input waveguide labelled follows a multiplexing stage where two input channels are added by coupling them to the TE_{00} and TE_{01} modes. The two modes then interact with the ring resonator via a directional coupler. If the mode is resonant in the ring it will be coupled to the drop port, if not the signal will pass to the through port. A demultiplexing stage is included after both the through and drop ports to recover the two channels separately for analysis. In the example provided in Fig. 1 the TE_{01} mode is resonant in the ring, while the TE_{00} mode is not. The transfer function at the drop port of the resonator (T_{drop}) can be described using (1) for any mode in the ring [11].

$$T_{drop} = \frac{P_{drop}}{P_{in}} = \frac{-\alpha\kappa^4}{2\alpha t^2\cos(\theta) - (\alpha^2 t^4 + 1)} \tag{1}$$

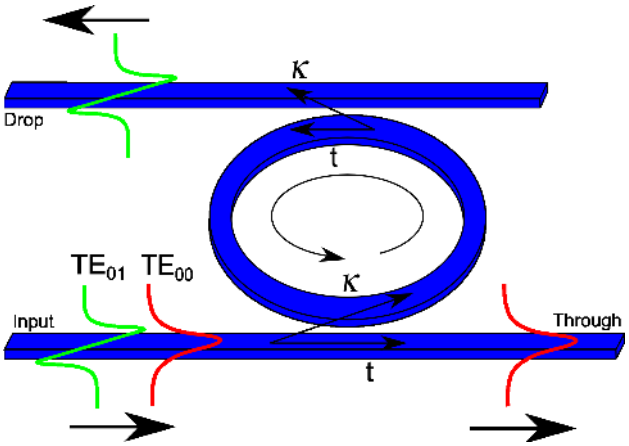

Fig. 1. A ring resonator composed of waveguides supporting two TE modes. In this example, the first-order mode (TE_{01}) is resonant and critically coupled to the drop port of the filter, while the fundamental mode (TE_{00}) is off resonance and passes to the through port.

Here, α is the attenuation factor of the mode after one revolution of the ring (where $\alpha = 1$ represents no attenuation), and θ represents the phase induced by the revolution. P_{drop} is defined as the power measured at the drop port, and P_{in} is the power at the input. The directional couplers between the ring and the add/drop ports are described by κ and t, the coupling and transmission coefficients of the electric field, respectively. In a lossless directional coupler these are related such that $t^2 + \kappa^2 = 1$. It can be seen in (1), when $\theta = 2\pi n$, where n is an integer, the mode is on

#201705 - $15.00 USD Received 21 Nov 2013; revised 17 Jan 2014; accepted 19 Jan 2014; published 20 Feb 2014

resonance and transmission at the drop port approaches a maximum determined by the value of α. The modes TE_{00} and TE_{01} have different effective refractive indices (n_{eff}), and therefore will become resonant in the ring at different wavelengths. This produces slightly different periodicities in the wavelength response of the filter. Another difference in the response of the two modes is seen in the directional coupler. The evanescent field of the TE_{01} mode extends much further into the cladding than the TE_{00} evanescent field. The coupling coefficients κ and t are heavily dependant on the overlap of the evanescent fields between the two waveguides, therefore the lengths for complete coupling (L_c) for each mode can differ by nearly an order of magnitude depending on the waveguide separation. The result of this difference has the largest effect on the quality factor (Q) of the resonator defined in (2), where L_{eff} is the effective length of the ring, and λ_0 is the center wavelength which is set to 1550 nm here [11].

$$Q = \frac{\pi L_{eff} n_{eff}}{\lambda_0 \arccos\left(\frac{1+t^4\alpha^2-4t^2\alpha}{-2t^2\alpha}\right)} \tag{2}$$

It is often desirable for the individual channels on a waveguide to have a similar response in devices such as filters. In many cases it would be ideal for the two modes to have near equal Q factors. Therefore, the κ and t values should be matched for TE_{00} and TE_{01}. Although Q is also dependant on n_{eff}, this value differs much less between modes. By considering directional coupler lengths (L) greater than the coupling length for TE_{01}, one can achieve equal κ values. The general expressions for calculating κ for each mode are presented in (3) and (4).

$$\kappa^{TE00} = \sin\left[\frac{\pi}{2}\left(\frac{L}{L_c^{TE00}}\right)\right] \tag{3}$$

$$\kappa^{TE01} = \sin\left[\frac{\pi}{2}\left(\frac{L}{L_c^{TE01}}\right)\right] \tag{4}$$

L_c^{TE00} and L_c^{TE01} are the coupling lengths for the TE_{00} and TE_{01} modes, respectively. In (5), κ^{TE00} is set equal to κ^{TE01}, where the range of L considered is $L_c^{TE01} < L < L_c^{TE00}$.

$$\sin\left[\frac{\pi}{2}\left(\frac{L}{L_c^{TE00}}\right)\right] = \sin\left[\pi - \frac{\pi}{2}\left(\frac{L}{L_c^{TE01}}\right)\right] \tag{5}$$

Solving (5) we find an analytic solution for L, which is displayed in (6).

$$L = \frac{2L_c^{TE01}L_c^{TE00}}{L_c^{TE00}+L_c^{TE01}} \tag{6}$$

Using this expression, a single length of coupler (L) can be found resulting in equal κ, with similar Q for the two modes. A disadvantage of this method is that for a fixed directional coupler geometry only one κ value is possible, which may be suitable for specific applications. However, it is possible to adjust the geometry of the directional couplers by tuning the waveguide widths or the gap between waveguides, which changes where κ is equal for both modes. In Fig. 2 the common coupling value for the two modes ($[\kappa^{TE00}(L)]^2$ and $[\kappa^{TE01}(L)]^2$) is plotted as a function of directional coupler gap for two waveguide widths. The values are calculated using (3) and (4) for a directional coupler of length L, which was calculated using (6). From this plot it is clear that only modest control over the coupling in the directional coupler is possible by adjusting these two parameters. For two-mode waveguides 980 nm wide, with a gap of 200 nm between them, 95 μm long directional couplers were found to produce 13.4% coupling (κ^2) for each mode.

#201705 - $15.00 USD Received 21 Nov 2013; revised 17 Jan 2014; accepted 19 Jan 2014; published 20 Feb 2014

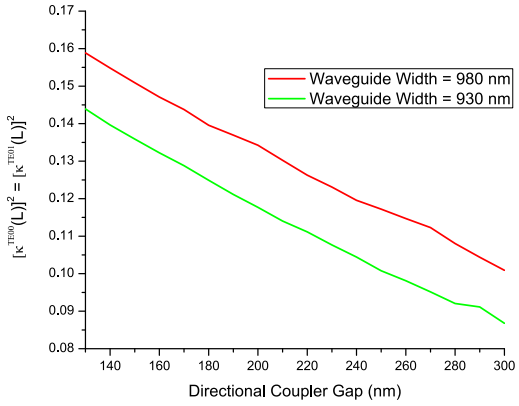

Fig. 2. The common κ^2 value for TE_{00} and TE_{01} in a directional coupler of length L. The directional coupler gap and waveguide widths are varied to demonstrate that some control over the equal κ^2 values can be achieved. During simulations the waveguide height and wavelength used were 220 nm and 1550 nm, respectively.

3. Multiplexing and demultiplexing

In order to demonstrate the multimode ring resonator, a reliable device for multiplexing and demultiplexing the TE_{01} mode is required. Many designs have been proposed to achieve this, including Y-junctions [12] and multimode interferometers (MMIs) [13]. Ultimately these designs were avoided as they cannot be easily extrapolated to multiplexing more than two channels, which would likely be a requirement in future MDM systems. Recently grating-assisted couplers have been proposed, which can multiplex several channels by adjusting the period of the grating between the input and bus waveguides [14]. The disadvantages of this design is a small bandwidth and relatively long coupling lengths. Asymmetrical directional couplers (ADCs) provide a good compromise for multiplexing, as they are easily cascaded for any number of modes [2], and are not strongly wavelength dependant. In wire waveguides ADCs have been shown to achieve (de)multiplexing on-chip while only occupying small fractions of the valuable chip space [2, 15]. The ADC concept requires a single-mode input waveguide that is phase matched to the desired higher-order mode in the bus waveguide [16]. In our case the phase matching we desired occurred between TE_{00} of the input waveguide and TE_{01} of the bus waveguide, which meant designing at widths that ensured the n_{eff} of each mode were equal. It is generally accepted that directional couplers exhibit poor fabrication sensitivity, but this has been overcome in many ways by introducing a linear taper in the bus waveguide [15]. A schematic of the tapered ADC design is shown in Fig. 3, where the width of bus waveguide increases linearly along the length of the ADC. For $W_1 = 450$ nm, it was found that W_2 must be 930 nm to satisfy the phase matching condition. The gap between waveguides, g, is maintained at 200 nm. The value of t is 50 nm for the tapered design, and reduced to 0 nm for the uniform case. The variable L_{ADC} represents the length of device for maximum coupling, which changes with the value of t.

Both the tapered and uniform ADC multiplexer designs have been simulated, and the results are shown in Fig. 4. The eigenmode expansion (EME) method available in FIMMWAVE®, and the finite-difference time-domain (FDTD) method available in Lumerical® were both used to simulate the device and agree quite well. Fig. 4(a) predicts the tapered ADC design will require

#201705 - $15.00 USD Received 21 Nov 2013; revised 17 Jan 2014; accepted 19 Jan 2014; published 20 Feb 2014

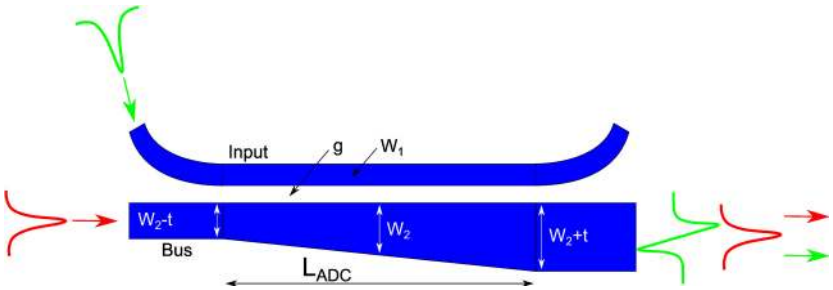

Fig. 3. The layout and operation of the ADC multiplexer design. Here W_1 and W_2 are the widths of the ADC input and bus waveguides, respectively; t is the thickness offset of the bus waveguide; g is the gap between the two coupler waveguides.

a longer length and produce a lower peak coupling in return for a much broader coupling peak with respect to length. Theoretically perfect coupling is not possible in the tapered ADC, as it is in the uniform ADC, because the phase matching condition is only met locally along the device. Note that the ADC input and output bends were not simulated with the EME method, which is why it appears to predict slightly longer lengths than FDTD. The tapered design is also found to achieve reduced sensitivity to fabrication errors, as demonstrated in Fig. 4(b). Error is simulated by increasing the waveguide widths (W_1 and W_2) by the error value, and by decreasing g by the error value. This method of defining error is meant to simulate how fabrication imperfections would affect the performance of a real ADC device. It can be seen that the taper allows approximately $\pm$ 50 nm in error while maintaining 3 dB coupling, where the uniform design allows for only $\pm$ 20 nm. As the fabrication of the ring resonator would require a total of three (de)multiplexers, the tapered ADC design was chosen to improve consistency.

After the demultiplexing stages of the device, the bus waveguides were tapered down to 500 nm where they became single-mode. The waveguide was also bent through 90° several times with a radius of 5 μm. This ensured that any residual TE_{01} mode not coupled out of the bus waveguide in the demultiplexer would be radiated out of the waveguide, further reducing crosstalk.

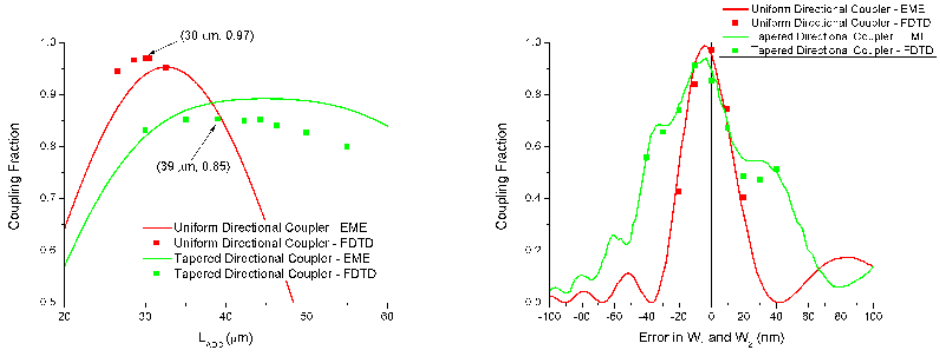

(a) (b)

Fig. 4. The coupling efficiency of tapered and uniform asymmetric directional couplers. FDTD and EME simulations are used to plot coupling fraction against (a) device length, and (b) fabrication errors in W_1 and W_2.

#201705 - $15.00 USD Received 21 Nov 2013; revised 17 Jan 2014; accepted 19 Jan 2014; published 20 Feb 2014

4. Ring bends

To ensure the free spectral range (FSR) of the filter is sufficiently large for filtering applications, a ring bend radius (R) of 20 μm or less was desired. However, the mode profiles in a bent waveguide of this radius differ significantly from those in a straight waveguide. The result is that when the two waveguides are connected mode mismatch at the interface will occur, leading to crosstalk between channels. The magnitude of this crosstalk has been calculated using the EME method, and is presented in Fig. 5 for radii of curvature up to 20 μm. Here, periodic dips in crosstalk are noticed as a function of radius, which is due to self-imaging within the bend [17]. At specific radii the length of the bend will be equal to $2L_\pi$, where L_π is the beat length of the two confined modes in the waveguide [18]. This produces the exact optical profile that was initially incident on the interface, and therefore greatly reduces crosstalk. The periodicity of the dips in Fig. 5 was found to be $\sim$ 1.5 μm, which agreed with the theoretical periodicity of 1.45 μm calculated from the beat lengths. While it is tempting to reduce crosstalk by simply choosing the ring resonator bend radius at one of the crosstalk dips, this was not pursued as the self-imaging condition is too wavelength dependant. It can be seen in Fig. 5 that away from the self-imaging dips the crosstalk levels are above the standard -20 dB required for many commercial applications.

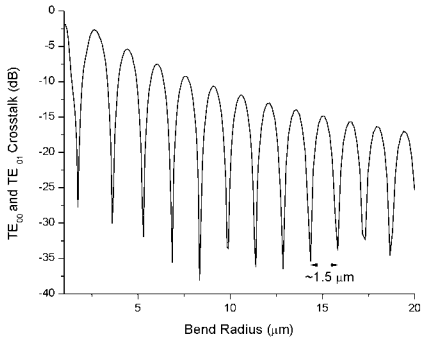

Fig. 5. Crosstalk between the TE_{00} and TE_{01} modes in a semi-circular waveguide connected to straight waveguides. Beating is noticed in the crosstalk response, which is attributed to self-imaging in the bend. Data was obtained using the EME method.

Another approach to reducing crosstalk in the ring bend is to remove the mode mismatch at the interface. This was achieved using transformation optics to design a bent waveguide with mode profiles that matched that of the straight waveguide [19]. Grayscale lithography was required to fabricate these waveguides, making them unsuitable for most applications. To keep fabrication relatively simple, we chose to replace the abrupt straight-to-bend transition using circular curves with an adiabatic curve. The adiabatic curve uses a gradual change in radius which acts to minimize conversion between modes. This is analogous to the adiabatic taper in fibers, which avoids modal conversion by narrowing the waveguide over a relatively long distance [20]. Adiabatic performance has been shown to exist in Bezier curves, which have been previously implemented in SOI waveguide devices [21]. Original work on Bezier curves focused only on reducing loss in single-mode wavguide bends [21]. In this work we study the reduction of crosstalk when using the adiabatic Bezier curves in our two-mode wavguide bends.

Bezier curves are typically defined by 4 points. For the 90° bends in [21], the start and end points are set to be $(0,0)$ and (R,R), respectively. The next two points then characterize how the

#201705 - $15.00 USD Received 21 Nov 2013; revised 17 Jan 2014; accepted 19 Jan 2014; published 20 Feb 2014

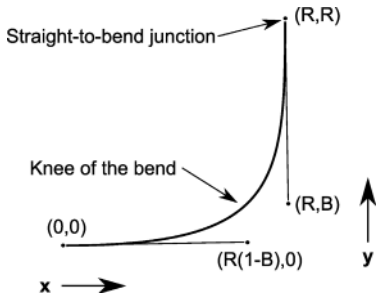

Fig. 6. The construction of the 90° Bezier curve. In the image the four points defining the curve, as well as the curve itself are displayed.

bend travels from the start to the end, and were defined as $(R(1-B),0)$ and (R,B). The mathematical construction is demonstrated in Fig. 6 [22]. The unitless parameter B was optimized to reduce crosstalk for our MDM application. A selection of the Bezier curves simulated are shown in Fig. 7(a). It can be seen that when B = 0.45, the curve closely resembles a circle where the transition between straight and bent waveguides is abrupt. In contrast, at B = 0.05 there is a very gradual change in radius at the interface, but a small radius near the knee of the bend. The crosstalk levels after propagating through a 90° Bezier curve were found using FDTD simulations, and are shown in Fig. 7(b). To remove the effects of self-imaging in the results of Fig. 7(b), the crosstalk levels were chosen from the peak value over a wide wavelength range of 100 nm, from 1500 to 1600 nm, over which two self-imaging instances are observed. We notice that the ideal value of B is consistently less than 0.45 regardless of the radius considered. We can therefore conclude that Bezier curves effectively mitigate crosstalk compared with circular curves. For our desired radius of 20 μm, B = 0.15 returned a crosstalk value of -41.9 dB, which is considered sufficiently low for communication applications. We note that the Bezier curve design has a great deal of potential for reducing crosstalk in any bend within a MDM system.

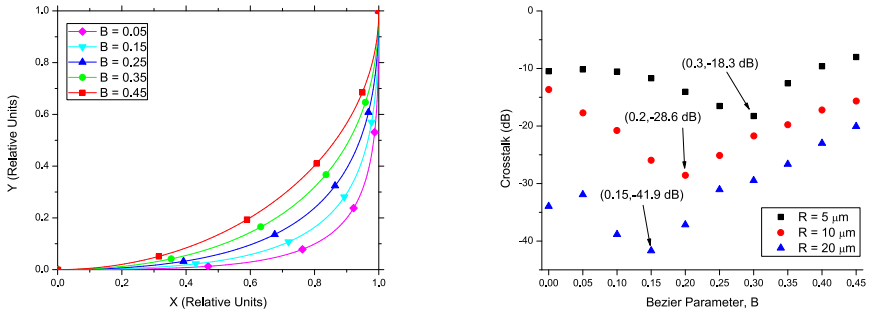

(a) (b)

Fig. 7. The design of adiabatic Bezier curves: (a) shows the shape of the bends for various values of B, and (b) shows the corresponding level of crosstalk in a 90° bend simulated using FDTD.

#201705 - $15.00 USD Received 21 Nov 2013; revised 17 Jan 2014; accepted 19 Jan 2014; published 20 Feb 2014

5. Experimental results

Our multimode ring resonators were fabricated onto 220 nm thick SOI wafers. Light was coupled to and from the chip using grating couplers [23]. In Fig. 8 a layout of the fabricated device is displayed. The input and output grating couplers are shown, along with all important device components and dimensions. The single-mode waveguides connecting the grating couplers to the (de)multiplexers were 450 nm wide, while the multimode waveguide sections were 980 nm wide. A 200 nm gap was used in all directional coupler configurations. The testing set-up employed for the measurements made use of a 3-channel fiber array with one input and two outputs. The fiber array coupled to the grating couplers displayed in Fig. 8 for light injection and collection. The middle fiber channel served as the input, while the other two fiber channels served as the through and drop port outputs. One measurement was done for the TE_{01} mode using the grating coupler array on the far left, and one was done for the TE_{00} mode using the grating coupler array to the right. Ideally, the measurements would have been performed with two, 3-channel fiber arrays, using one for each mode. Crosstalk measurements could then be performed by exciting either the TE_{00} or TE_{01} channel and observing the outputs of the other channel. However, such measurements would increase the complexity of the testing set-up and increase the footprint of the device. For the ease of measurement, crosstalk levels were obtained from two identically designed rings fabricated on the same wafer as the original device. The grating couplers in these devices were rearranged so that input for the TE_{00} mode was aligned with the TE_{01} mode outputs, and likewise for the TE_{01} mode input. To demonstrate the resonance response of the filter a wavelength sweep over 20 nm (from 1540 to 1560 nm) was performed during testing, however in actual device operation a single operating wavelength would be used.

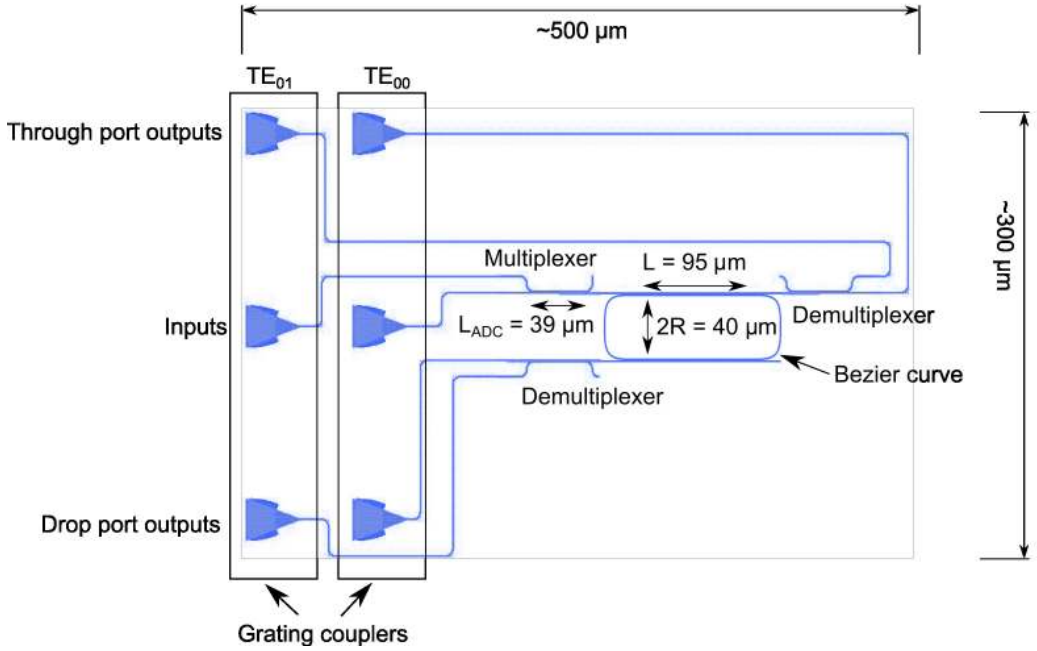

Fig. 8. The multimode ring resonator mask layout used for fabrication. The different components and dimensions of the device are labelled.

The optical output from the through and drop ports is presented in Fig. 9. The data here

#201705 - $15.00 USD Received 21 Nov 2013; revised 17 Jan 2014; accepted 19 Jan 2014; published 20 Feb 2014

clearly displays unique resonances for the TE_{00} and TE_{01} modes. A second identically designed ring was fabricated on the same wafer. It was found that the resonance peaks of this device were shifted by ∼0.3 nm compared to the peaks presented in Fig. 9 for each mode, indicating that fabrication defects will have a modest effect on resonant wavelengths. The crosstalk results from one device are also shown in Fig. 9. Here, TE_{01} XT is the optical power measured from the TE_{01} output when a TE_{00} mode is input into the ring, and likewise for TE_{00} XT. We summarize the properties of both modes within the ring resonator device in Table 1 over the 20 nm wavelength range displayed in Fig. 9.

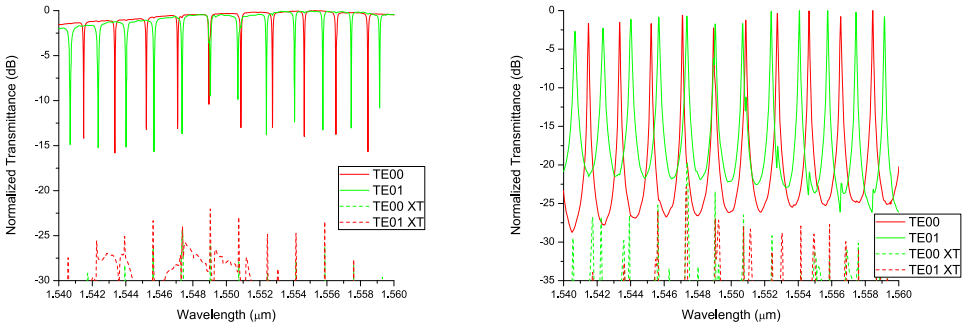

Fig. 9. Normalized optical output for the TE_{00} and TE_{01} modes from (a) the through port, and (b) the drop port. Crosstalk (XT) results are also presented.

Table 1. Theoretical and experimental properties of the TE_{00} and TE_{01} modes in the multimode ring resonator. The wavelengths considered range from 1.54 μm to 1.56 μm.

Property	TE_{00}	TE_{01}
Through port loss (exp.)	12 dB	15 dB
Drop port loss (exp.)	15 dB	19 dB
Minimum SXR at the through port (exp.)	24 dB	22 dB
Minimum SXR at the drop port (exp.)	18 dB	23 dB
Through port extinction ratio (exp.)	13 dB	12 dB
Drop port extinction ratio (exp.)	25 dB	20 dB
FSR (simulated)	1.896 nm	1.692 nm
FSR (exp.)	1.90 nm	1.68 nm
Q (exp.)	22 000	26 000

When comparing the fiber-to-fiber loss of the TE_{00} and TE_{01} modes from Table 1, we notice that the trends are consistent with both theory and previous work. Since coupling inefficiencies in the grating couplers account for approximately 10.5 dB of loss [23], we can conclude that the loss of the TE_{00} mode at the through port is largely attributed to the grating couplers. The TE_{01} mode experienced about 3 dB more loss than the fundamental mode from two additional sources. First, incomplete coupling at the multiplexers and demultiplexers reduces the power of only the TE_{01} mode. From separate measurements of the ADC multiplexers and demultiplexers, we calculated an average loss of 1.25 dB per (de)multiplexer. Therefore, the ADCs account for approximately 2.5 dB of the additional loss observed in the TE_{01} mode. The second source

#201705 - $15.00 USD Received 21 Nov 2013; revised 17 Jan 2014; accepted 19 Jan 2014; published 20 Feb 2014

of loss is increased sidewall scattering, as the optical power for this mode extends further in the horizontal direction compared to TE_{00}, resulting in a larger overlap with the waveguide sidewalls. Assuming 10.5 dB of loss in the grating couplers, and 2.5 dB of loss in the ADCs for the TE_{01} mode, we calculate the propagation losses of the TE_{00} and TE_{01} modes at the through port to be 1.5 dB and 2 dB, respectively. In the case of the drop port, the loss of the modes is 3 and 4 dB higher than at the through port, for the TE_{00} and TE_{01} modes, respectively. The ring resonator has not satisfied the condition for critical coupling for either mode, which accounts for some reduced output power at the drop port during resonance [7]. To achieve critical coupling in the add/drop ring resonator, the coupling at the through port must match the loss in the ring plus the coupling at the drop port, such that $\kappa_{through} = (1-\alpha) + \kappa_{drop}$, for each mode. This condition for single-mode rings is well known for directional coupler gaps of $g_{through} < g_{drop}$. In our case the critical coupling condition would need to be satisfied for both modes, making it much more difficult to achieve. Propagation within the ring is another expected source of the increased loss. The loss should be higher for the TE_{01} mode once again due to additional sidewall scattering.

We see that the signal-to-crosstalk ratio (SXR) at the drop port of the ring resonator device is larger than what we expected from mode mismatch in the Bezier curves of Fig. 7(b). However, the result is not surprising as fabrication defects such as waveguide sidewall roughness present an additional source of crosstalk not included in simulations. Imperfections at the waveguide edges can couple the two modes regardless of how the waveguide is designed. Although simulations predict very low levels of crosstalk from the ADC (de)multiplexers (SXR $>$ 30 dB), fabrication defects decreased the measured SXR from six ADC devices tested separately to an average of 23.9 dB. Additional ring resonator crosstalk measurements, which are not displayed in Fig. 9, also demonstrated a SXR above 18 dB for both modes and all output ports. These results agree with the results presented in Fig. 9 and Table 1, indicating there are no significant fluctuations in overall crosstalk performance between the two devices. By omitting that single isolated spike in crosstalk for the TE_{00} mode at the drop port in Fig. 9, we can see that the SXR is roughly equal at both the through and the drop ports. Theoretically, the ring bends will have very little effect on the SXR of the through port, as the light does not resonate and build up intensity in the ring. Therefore, we can conclude that the Bezier curves were not the largest contributor to crosstalk in the system. It is likely instead that the fabrication defects were the dominating source of mode conversion, as it would affect the SXR of the through and drop ports almost equally.

The distinct values of n_{eff} for each mode explains the slightly different FSRs we notice in both simulations and experiments. The excellent agreement between simulated and experimental FSRs confirms that we have witnessed the resonance response of the TE_{00} and TE_{01} modes as intended. From (2) we expect TE_{00} to have a higher Q value than TE_{01} based on its higher n_{eff}, assuming κ is equal for both modes. As well, TE_{01} has a higher loss which would also reduce the Q value for this mode. However, this is not the case in our experimental results. Therefore we speculate that the TE_{00} mode had slightly stronger coupling in the directional coupler compared to TE_{01}, reducing the Q value. Table 1 also compares the extinction ratios for both modes at the through and the drop port. The low values for extinction ratio ($<$15 dB) at the through port again indicates that the critical coupling condition has not been met for either mode. At the drop port however, the filter exhibits much larger extinction ratios. We therefore conclude that the coupling and loss within the ring is better optimized at this port near the 1550 nm wavelength.

By inspecting the results of Fig. 9, a wide range of applications become clear for this device. The slightly different FSR for each mode allows one to design the ring resonator to selectively filter one or more specified modes. From the wavelength response of the filter it is clear that

#201705 - $15.00 USD Received 21 Nov 2013; revised 17 Jan 2014; accepted 19 Jan 2014; published 20 Feb 2014

filtering operation can be optimized for one specific mode, both modes, or no mode at all. For example, in a MDM system using this ring resonator at 1.549 μm, both modes are coupled to the drop port. This is a unique quality of the ring resonator in a MDM system, as the number of modal channels that are filtered can be designed for by adjusting the radius of the ring or the operating wavelength. The number of applications for the filter grow further when considering an active ring resonator design, such as those demonstrated in the past [7, 8]. Channel selective switching then becomes possible simply by adjusting the refractive index of the ring. As well, the switching would be in no way limited to a single channel at a time. Furthermore, the two-mode ring can be extended to support additional modes for MDM systems with larger channel numbers. There are no theoretical limits to the number of modes a MDM system can support, however practical limitations such as large waveguide widths leading to weak coupling for the fundamental mode will likely limit this kind of system to 5-10 modes. Matching the values of κ for many modes would add to the design challenge, however similar Q values may not be essential for every application, which would increase the level of freedom one has in the ring resonator design.

6. Conclusion

We have successfully demonstrated a two-mode division multiplexing ring resonator. From our results we conclude that each mode resonates independent of the other within the ring. Optimization of the ring parameters was performed so that similar responses were observed for each mode. We have compared two variations of the asymmetric directional coupler for use as the multiplexer and demultiplexer for the device. In the fabricated device a tapered design was employed as it demonstrated a resilience to fabrication errors. The interface between straight and bent waveguide sections was identified as a potential source of crosstalk in the design. Simulations and experiments both showed that the introduction of Bezier curves in the ring bends could mitigate the crosstalk. The signal-to-crosstak ratio in the ring stayed above 18 dB for both modes at the through and drop ports. We conclude that the ring resonator is an excellent channel selective filter for mode-division multiplexing (MDM) systems. Switching is also possible using rings by integrating refractive index tuning in the device.

Acknowledgments

The authors would like to thank CMC Microsystems and the University of British Columbia for their support in fabrication, which was done at the University of Washington Microfabrication/Nanotechnology User Facility. As well we thank CMC Microsystems for providing access to the simulation and design software. We acknowledge the inspiring work of L. Chrostowski and J. Flueckiger in the Bezier bend design, and Y. Wang for the fiber grating coupler design. Finally, we are grateful to V. Donzella who prepared the mask, R. Bojko for the fabrication, J. Flueckiger and C. Lin for the designing and constructing the experimental set-up, and Wyichen Wu for conducting the measurements.

#201705 - $15.00 USD Received 21 Nov 2013; revised 17 Jan 2014; accepted 19 Jan 2014; published 20 Feb 2014